Combining Generative Adversarial Network and First-Principles Based Microkinetics for Heterogeneous Catalyst Design

Atsushi Ishikawa [1,2,3*]

(*E-mail: ISHIKAWA.Atsushi@nims.go.jp)

[1] Center for Green Research on Energy and Environmental Materials (GREEN), National Institute for Materials Science (NIMS), 1-1 Namiki, Tsukuba, Ibaraki 305-0044, Japan

[2] PRESTO, Japan Science and Technology Agency (JST), 4-1-8 Honcho, Kawaguchi, Saitama 333-0012, Japan

[3] Elements Strategy Initiative for Catalysts & Batteries (ESICB), Kyoto University, Nishikyo-ku, Kyoto 615-8510, Japan

Abstract

Microkinetic analysis based on density functional theory (DFT) was combined with a generative adversarial network (GAN) to enable artificial proposal of heterogeneous catalysts based on the DFT-calculated dataset. The approach was applied to the NH_3 formation reaction on Ru-Rh alloy surfaces as an example. The NH_3 formation turnover frequency (TOF) was calculated by DFT-based microkinetics. Specifically, six elementary reactions (N_2 dissociation, H_2 dissociation, NH_x (x = 1–3) formation, and NH_3 desorption) were explicitly considered, and their reaction energies were evaluated by DFT. On the basis of TOF values and atomic compositions, new alloy surfaces were generated using the GAN. This approach successfully generated the surfaces not included in the initial dataset but have higher TOF values. The N_2 dissociation reaction was more exothermic for the generated surfaces, leading to higher TOF. The present study shows that automatic improvement of catalyst materials is possible by using the iterative steps of DFT calculation and sample generation by GAN.

1. Introduction

Catalysts play a crucial role in energy and environmental science, and its performance is often evaluated by the reaction rate or turnover frequency (TOF). Researchers have devoted great efforts to find new catalysts with higher reaction rates. It is well known that the reaction rate is governed by several factors: the activation energies, the number of active sites (or surface area of the catalyst), sticking coefficients on the surface, etc. Unfortunately, accurate measurement of such quantities requires both special expertise and great effort; therefore, detailed kinetic profiles have only been clarified for limited cases.

In the last few decades, theoretical simulation and computational methods became feasible alternatives to evaluate reaction kinetics. *Ab initio* or first-principles calculation is a popular one, because it provides atomic-scale information without requiring experimental data. For example, this approach can be helpful in identifying the active site on the catalyst surface, which is a fundamental issue in catalysis. Owing to recent developments in algorithms and computational resources, such atomic-scale simulations, especially those using density functional theory (DFT), are widely used nowadays.

While computational methods are useful for studying given real or proposed materials, it cannot automatically suggest new ones. Recently, it was realized that applying machine learning to computational chemistry could lead to computation-based material proposal.[1] Several promising examples have been reported in catalysis.[2-5] Among the several possibilities of combining computational chemistry and machine learning, the present author considers the so-called generative model a particularly important machine learning algorithm because it enables "extrapolative" proposal in the material or configuration space; that is, the search is not confined within given dataset. As a type of generative model, the generative adversarial network (GAN) is widely used, especially in artificial image generation.[6, 7] Several groups have reported the application of GAN to material science; Kim *et al.* used it to find new zeolite systems,[8] and several groups also used it to artificially generate crystal

structures with desirable properties.[9, 10]

A catalytic reaction often involves several species and elementary reactions. Microkinetic analysis explicitly treats a set of elementary reactions. Therefore, it is often more accurate than the kinetic analysis based on the global rate expression.[11] Currently, DFT-based microkinetics is widely used in catalysis research because it is a powerful tool since kinetic information, such as reaction energy and activation barrier, can be calculated by DFT.[11-15] Considering this, the combination of DFT calculations, microkinetics, and catalytic material generation from generative models is a promising approach toward the rational design of catalysts.

The present paper describes a new approach based on DFT calculations and sample generation by GAN for heterogeneous catalyst search. The generation procedure is extrapolative, because the proposed catalytic material need not be included in the initially prepared dataset. Here, the GAN part aims to generate materials with a high TOF for the target catalytic reaction, where the TOF is calculated using DFT-based microkinetics. The ammonia (NH_3) synthesis reaction, known as the Haber-Bosch process, is considered in this study as a representative heterogeneous catalytic reaction.[16-18] Below, details of the DFT-GAN procedure are described in the Methods section, and its performance is discussed in the Results and Discussion section.

2. Methods

a. Models and details of DFT calculation

Here, catalytic NH_3 synthesis is assumed to occur on a Rh-Ru bimetallic alloy surface. The Ru stepped surface was constructed first, and the bimetallic alloys were constructed by replacing Ru atoms with Rh atoms. Stepped metal surfaces were considered because NH_3 formation is known to occur there.[17, 19] The positions of the Ru atoms replaced by Rh atoms were chosen randomly in the original dataset, while the position of the Rh atoms is determined by the GAN; the details will be discussed later. The original dataset included 100 metal surfaces. The metal surfaces are modeled by repeated

slabs, and the stepped surface is modeled by removing half of the atoms in the top layer. Each slab consists of a (6×4) supercell in the lateral direction, with four atomic layers in the z-direction. Consequently, 84 atoms are included in the model. The typical structure of the surface model is shown in Fig. 1. The adsorption positions of N, H, NH, and NH_2 were assumed to be the fcc three-fold hollow site and atop adsorption was assumed for NH_2 and NH_3, as these positions are the most stable adsorption sites on the Ru-stepped surface.[20] These adsorption sites are shown in Fig.1.

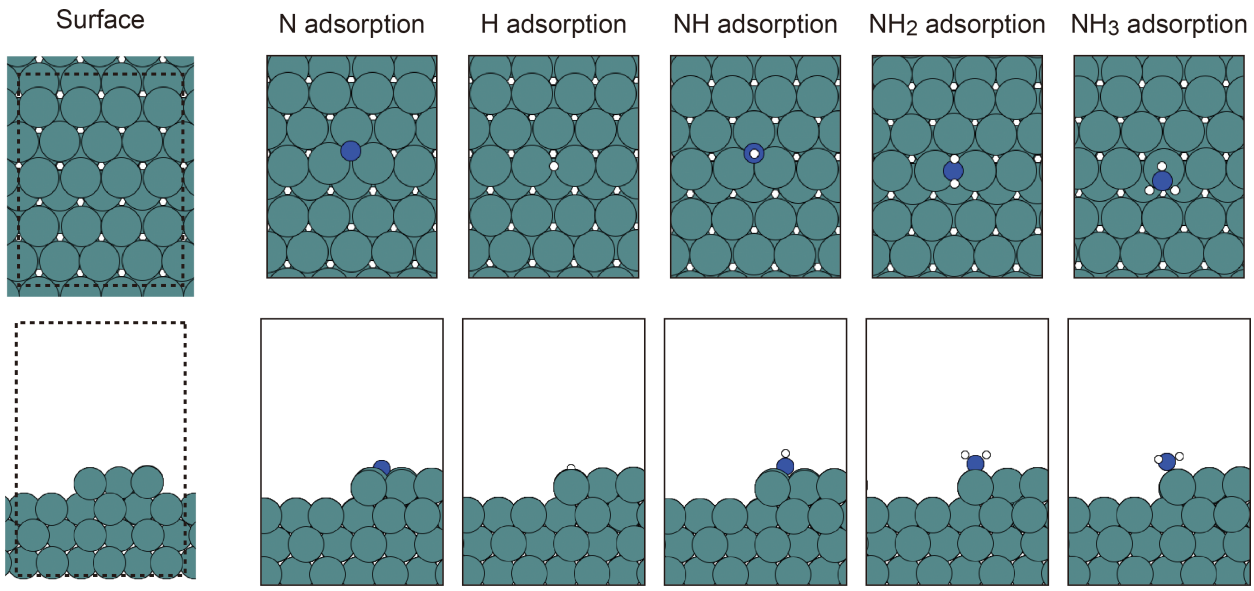

Figure 1. Typical slab model for the stepped surface, and the adsorption sites of the N, H, NH, NH_2, and NH_3 species. The upper and lower panels are top and side views. The dotted line in the bare surface model shows the boundary of the supercell. The metal, N, and H atoms are shown in gree, blue, and white spheres, respectively.

The BEEF-vdW exchange-correlation functional was used in the DFT calculations because it provides an accurate description of the van der Waals interaction.[21] The core electrons were represented by the projector-augmented wave (PAW) potentials.[22] The valence electrons were expanded with plane waves up to a cutoff energy of 400 eV. Spin polarization was included throughout, and no symmetry constraint was imposed on the geometries. A Gaussian scheme was used in the smearing of electron occupation near the Fermi level. The convergence thresholds for the electronic and geometry

optimizations were set to 1.0×10^{-4} eV and 1.0×10^{-1} eV/Å in energy and force, respectively. Optimization of the unit cell lengths was performed for all surfaces in the absence of the adsorbate molecules. Brillouin zone integration was performed by numerical integration at the gamma point. A vacuum layer of ~12 Å was placed between the slabs, and dipole correction was applied in the z-direction to cancel the artificial interaction between slabs. All DFT calculations were performed using the Vienna *ab initio* simulation package (VASP) version 5.4.4.[23, 24]

b. Elementary reactions and rate of NH_3 formation

The overall reaction of NH_3 synthesis

$$N_2 + 3H_2 \rightarrow 2NH_3 \quad (1)$$

is generally considered to include the following six elementary reactions.[25]

$$N_2 + 2* \rightarrow 2N* \quad (2)$$

$$H_2 + 2* \rightarrow 2H* \quad (3)$$

$$N* + H* \rightarrow NH* \quad (4)$$

$$NH* + H* \rightarrow NH_2* \quad (5)$$

$$NH_2* + H* \rightarrow NH_3* \quad (6)$$

$$NH_3* \rightarrow NH_3 + * \quad (7)$$

where the asterisk (*) denotes a vacant active site on the metal surface, and the species with asterisks are the adsorbed species. The reaction energies in eq. (2)–(7) were determined from the total energy calculated by DFT, that is, the sum of electronic and nuclear repulsion energies.

Previous experimental and theoretical work suggests that the rate-determining step (RDS) is eq. (2), namely the dissociative adsorption of N_2.[17, 26] The present study followed this assumption, and the other reaction steps were equilibrated. In this case, the fractional surface coverage of adsorbed species i (θ_i) is written as

$$\theta_{\mathrm{N}} = \frac{p_{\mathrm{NH_3}}}{K_3^{3/2} p_{\mathrm{H_2}}^{3/2} K_4 K_5 K_6 K_7} \theta_{\mathrm{vac}}$$

$$\theta_{\mathrm{H}} = \sqrt{K_3 p_{\mathrm{H_2}}}\, \theta_{\mathrm{vac}}$$

$$\theta_{\mathrm{NH}} = \frac{p_{\mathrm{NH_3}}}{K_3 p_{\mathrm{H_2}} K_5 K_6 K_7} \theta_{\mathrm{vac}}$$

$$\theta_{\mathrm{NH_2}} = \frac{p_{\mathrm{NH_3}}}{\sqrt{K_3 p_{\mathrm{H_2}}} K_6 K_7} \theta_{\mathrm{vac}} \tag{8}$$

$$\theta_{\mathrm{NH_3}} = \frac{p_{\mathrm{NH_3}}}{K_7} \theta_{\mathrm{vac}}$$

$$\theta_{\mathrm{vac}} = \frac{1}{1 + \frac{p_{\mathrm{NH_3}}}{K_3^{3/2} p_{\mathrm{H_2}}^{3/2} K_4 K_5 K_6 K_7} + \sqrt{K_3 p_{\mathrm{H_2}}} + \frac{p_{\mathrm{NH_3}}}{K_3 p_{\mathrm{H_2}} K_5 K_6 K_7} + \frac{p_{\mathrm{NH_3}}}{\sqrt{K_3 p_{\mathrm{H_2}}} K_6 K_7} + \frac{p_{\mathrm{NH_3}}}{K_7}}$$

where p_i is the partial pressure of NH_3 or H_2, and K_i is the equilibrium constant of eqs. (2)–(7).[25] Then, the total reaction rate is written as

$$R = k \cdot p_{\mathrm{N_2}} \theta_{\mathrm{vac}} \left(1 - \frac{1}{K_2 K_3^{3} K_4^{2} K_5^{2} K_6^{2} K_7^{2}} \frac{p_{\mathrm{NH_3}}^{2}}{p_{\mathrm{N_2}} p_{\mathrm{H_2}}^{3}} \right) \tag{9}$$

where k is the rate constant of RDS (eq. (2)) calculated using the Arrhenius equation:

$$k = A \exp\left(-\frac{E_a}{RT} \right). \tag{10}$$

E_a is the activation energy of eq. (2), A is the pre-exponential factor with the value of 0.241 s^{-1} given by Logadottir *et al.*,[20] R is the universal gas constant, and T is the temperature. For the zero-point energies and thermal correction terms, experimental values from the NIST webbook were used. [27]

Although it is possible to evaluate E_a with DFT by locating the transition state, this process requires considerable computational effort. Instead, this study evaluated E_a using the linear free energy relationship (or the Bronsted-Evans-Polanyi principle), in which E_a is expressed as a linear function of ΔE as

$$E_a = \alpha \Delta E + \beta. \tag{11}$$

The values of $\alpha = 0.87$ and $\beta = 1.34$ for the stepped metal surface were taken from the literature.[28] The

calculation was carried out at T = 700 K and a total pressure of 100 bar. N_2 and H_2 in the inlet gas were stoichiometric, *i.e.*, $p_{N_2} : p_{H_2} = 1 : 3$. The conversion of N_2 was set to 10%.

c. Details of the GAN

Similar to the original and several extended versions of GAN, the entire system here consists of the generator (G) and discriminator (D) networks. In the present case, fake samples with a high NH_3 formation rate are desirable, and they can be generated using G. Therefore, the conditional GAN (CGAN) was applied because it enables the generation of fake samples corresponding to a given label.[7] The structures of G and D are shown in Figure 2. The metal surface is encoded by a one-dimensional string array consisting of Rh or Ru. Then the string is converted to the one-dimensional vector of either 0 or 1 value. This vector and the DFT-calculated TOF value are used as the descriptor and target values, respectively. These alloys and their DFT-calculated TOF values were used together for learning. The mean squared error is used for the loss function of D and G parts.[29] Because the fake samples are expressed as a one-dimensional vector of transition metal elements and the initial atomic positions, DFT calculations can be carried out for these samples. This also means that their NH_3 formation rates could be evaluated with the same accuracy as the original dataset. DFT calculation results for the generated samples were added to the original dataset, and the augmented dataset was used for iterative training of the GAN. The specific steps are as follows:

(1) DFT calculation is performed to obtain E_a and ΔE values for elementary reactions of eq. (2)–(7). This is done for all samples in the dataset.

(2) The TOF for NH_3 formation is calculated according to eq. (9) using the DFT-calculated ΔE and E_a values.

(3) The calculated samples are sorted according to the DFT values and grouped into several classes (n) according to the NH_3 formation rate. Here, the number of groups is set to five, and the group with the highest TOF is labeled n = 1.

(4) Networks D and G are trained with the dataset using the backpropagation scheme.

(5) G generates fake samples for n = 1. Any generated surface that overlaps with the existing sample set is removed.

(6) DFT calculation is performed for the newly generated samples. The results are added to the dataset for use in the next iteration.

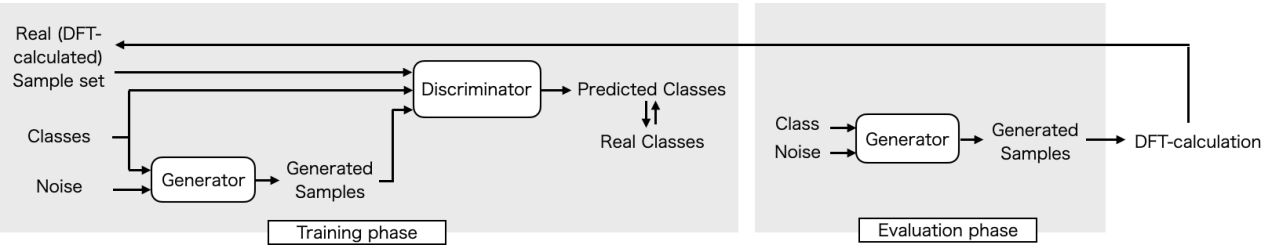

Figure 2. Structure of the DFT-GAN procedure used in this work. In the training phase, the generator and discriminator are trained using DFT-calculated data. Then, new samples are generated in the evaluation phase. This training-evaluation sequence consists of one iteration. After the newly generated samples are evaluated by DFT calculation, they are added to the original dataset for use in the next iteration.

Note that the size of the dataset increases as the iterations proceed. This feature is favorable in terms of training neural networks, as a larger number of samples can be used in the training. Several studies have shown that such iterative training of the GAN is effective.[30, 31]

When training D and G, the loss function was set to the mean-squared error in both cases, and the ADAM optimizer was used. The learning rate was set to 1.0×10^{-3}, and the parameters β_1 and β_2 were set to 0.5 and 0.999, respectively. The dropout rate was set to 0.3. The minibatch size was set to 20% of the sample size at each iteration. The maximum number of the training process (*i.e.*, the epoch) was set to 2000.

The Python library atomic simulation environment (ASE) was used to construct the model and

perform the DFT calculations.[32] The GAN part was calculated with PyTorch version 1.8. These Python codes are freely available on the author's GitHub page.[33]

3. Results and Discussion

First, 100 bimetallic alloy surfaces were generated by randomly replacing Rh atoms with Ru atoms on a surface. DFT calculations were performed on these samples to obtain the TOF values. In the following, this dataset is called the "original dataset." Then, the iterative GAN procedure described above was applied. Five iterations were performed, meaning that four generations of new samples were created in addition to the original dataset.

Figure 3(a) plots the TOF of each metal surface on a logarithmic scale, and the surfaces are sorted in descending order of TOF. In the original dataset (iter = 0), the metal surfaces have a wide range of TOF values ranging from 1.0×10^{-4} (Rh_8Ru_{76}) to 2.3×10^{-19} $site^{-1} \cdot s^{-1}$ ($Rh_{50}Ru_{34}$). This indicates a strong dependence of TOF on the metal surface composition. The new metal surfaces generated by the first to fifth iterations of DFT-GAN (iter = 1–5) are shown in the figure. It can be seen that the generated surfaces tend to have relatively higher TOF values than the original dataset. At iter = 3, Rh_4Ru_{80} is generated, and it has a TOF value of 3.1×10^{-4} $site^{-1} \cdot s^{-1}$, which is higher than the maximum TOF in the original dataset. At iter = 5, the best TOF value (1.1×10^{-3} $site^{-1} \cdot s^{-1}$) is obtained with Rh_8Ru_{76}; this TOF value is more than ten times larger than the best value in the original dataset. These facts show that the GAN successfully generated a metal surface with high catalytic performance in an extrapolative manner. The TOF values at each iteration are summarized in the so-called violin plot in Figure 3(b). The violin-shaped curves show the probability density of the TOF values, and the box inside each curve indicates the quartiles. The plot shows that the original dataset has widely distributed TOF values. The TOF value distribution of the generated surfaces (iter = 1–5) are more skewed toward the high TOF region. This trend clearly shows that the GAN is much more efficient than the random sampling, to obtain the metal surface with high NH_3 formation rate.

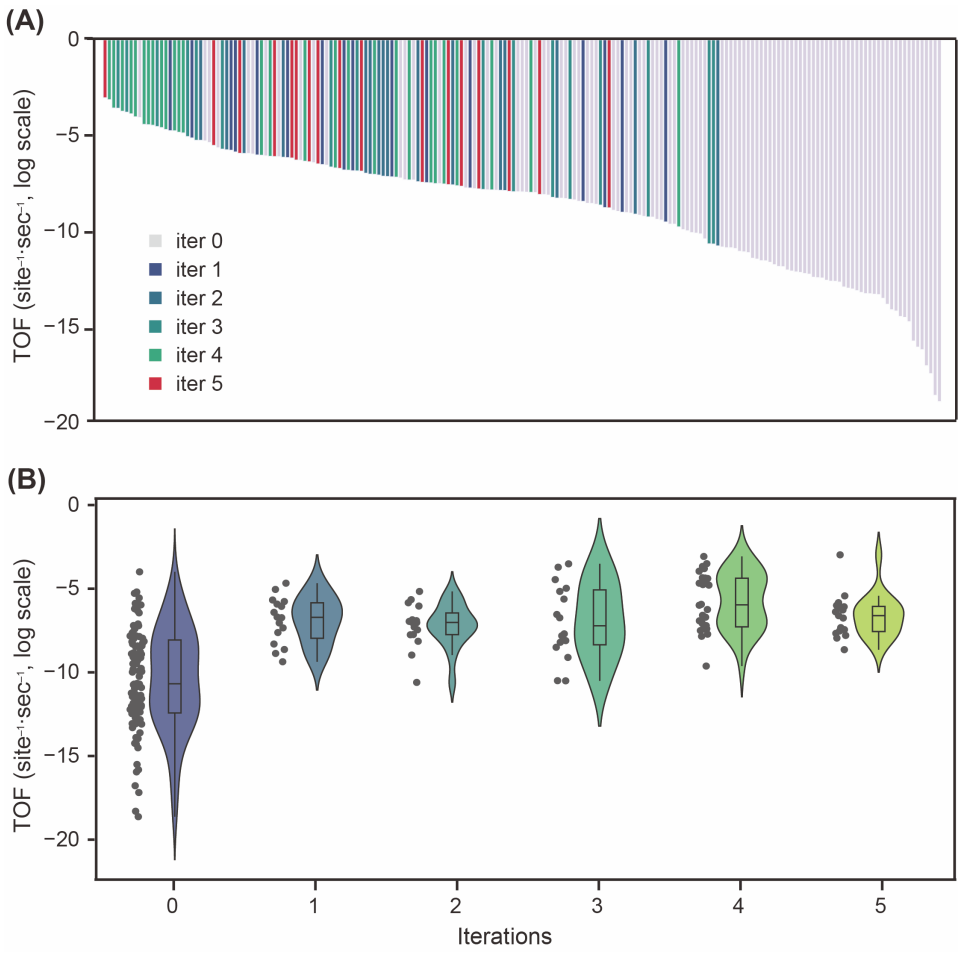

Figure 3. (a) TOF of NH_3 formation on 224 Ru-Rh alloy surfaces. The TOF values from different DFT-GAN iterations (iter = 1–5) are coded by different colors. The iter = 0 corresponds to the original dataset. The dataset is sorted according to the DFT value, from the highest (left) to the lowest (right). The reaction temperature and total pressure are 700 K and 100 bar, respectively. (b) The box and violin plots of the TOF values for iter 0–5. The line inside the box represents the median value. The points on the left of the violin represent the raw TOF value at each iteration.

The property of the generated surface agrees with the existing chemical or physical insights. It is widely known that NH_3 formation is much faster on the Ru surface than on the Rh surface.[34] In this study, surfaces generated by GAN tend to have a high proportion of Ru; the full dataset can be found in Supporting Information. This shows that the neural network captures the experimental tendency of transition metal elements by learning from the TOF of NH_3 formation calculated by DFT.

The generator loss (G-loss) and discriminator loss (D-loss) during the training process are plotted in Figure 4. Since each iteration has 2000 epochs, there are 10000 epochs in five iterations. At the earlier stage of training, G-loss is smaller than D-loss. However, after ~1000 epochs, D-loss becomes lower than G-loss, meaning that the D part of the GAN is well-trained.

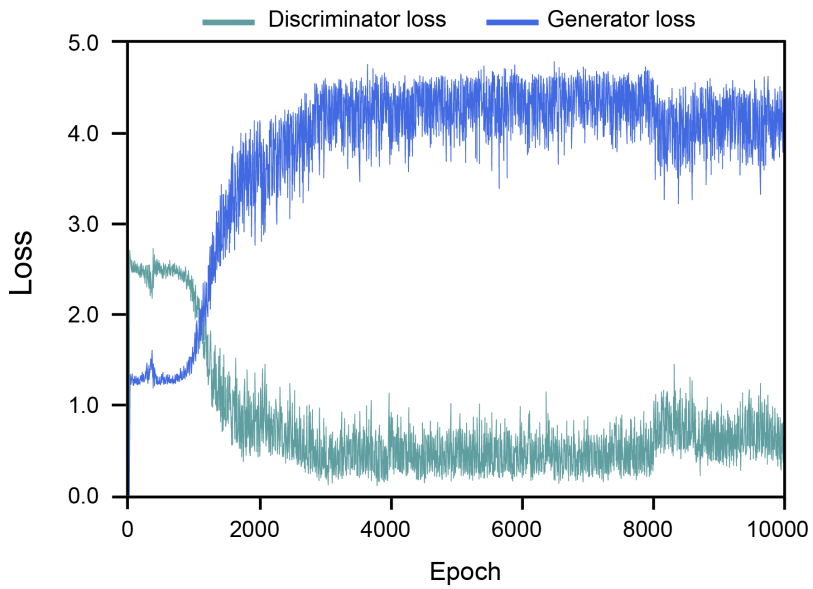

Figure 4. Discriminator and generator losses during the DFT-GAN procedure. Each iteration has 2000 epochs.

To understand why the generated surfaces have higher TOFs, the energetics of NH_3 formation reaction were analyzed. Figure 5 summarizes the potential energy curves, reaction energies of the elementary reactions, and surface fractional coverages of the adsorbates. Here, the Rh-Ru surfaces with the best TOF values at iter = 0, 3, 4, and 5 are compared. The compositions of these surfaces are Rh_8Ru_{76}, Rh_4Ru_{80}, $Rh_{12}Ru_{72}$, and Rh_8Ru_{76}, respectively. The best TOF value (1.1×10^{-3} site^{-1}·s^{-1}) is that of Rh_8Ru_{76}, which is generated at iter = 5. This value is much higher than that of Rh_8Ru_{76} at iter = 0 (1.0×10^{-4} site^{-1}·s^{-1}), which is the highest TOF in the original dataset (for brevity, these surfaces are denoted as Rh_8Ru_{76}-iter5 and Rh_8Ru_{76}-iter0 in the following discussion). Note that these two surfaces have the same composition, but the position of the Rh atoms are different each other.

Figure 5(a) plots the potential energy curves for NH_3 formation. Two NH_3 molecules are formed because the dissociation of one N_2 molecule generates two N* (surface-adsorbed N) atoms. The plots show a deep potential energy sink at the NH_2* + N* + 4H* state caused by the exothermic formation of NH and NH_2 and endothermic formation of NH_3. This energy sink is unfavorable from the thermodynamic viewpoint because the high stability of NH* and NH_2* leads to surface poisoning. The lack of vacancy in the active site prohibits the next catalytic reaction; this issue will be discussed later. The potential energy curves for iter = 2–4 have lower potential energy at NH_2* + N* + 4H*, similar to that for iter = 0. However, at iter = 5, the endothermicity of the reaction is much improved. This is beneficial in terms of the accessibility of the N_2 molecule on the active site. Thus, the potential energy curves show that the GAN-generated surfaces successively improve the thermodynamic character of NH_3 formation.

The reaction energies (ΔEs) of the elementary reactions (eq. (2)–(7)) on several surfaces are shown in Figure 5(b). The reaction energy of N_2 dissociation (eq. (2)) is more exothermic at iter = 2–5. For example, the ΔE on Rh_8Ru_{76}-iter5 is −0.79 eV, which is lower than that on Rh_8Ru_{76}-iter0 (−0.72 eV). Consequently, the activation barrier E_a becomes lower in the latter owing to the linear free energy relationship (eq. (11)). Another notable feature is the ΔE for NH_3 formation. As stated above, the facile formation of NH_3 alleviates surface poisoning by NH_2. The Figure 5(b) shows that ΔE for NH_3 formation progressively becomes less endothermic as the iteration proceeds. This suggests that the GAN improves not only the kinetics but also the thermodynamics of the NH_3 formation.

Figure 5(c) compares the fractional coverage (θ) of different adsorbates (N, H, NH, NH_2, and NH_3) and the vacant site (*i.e.*, the active site) over several Rh-Ru surfaces. A notable difference is seen in the coverage of vacant site (θ_{vac}); for example, θ_{vac} is 7.5×10^{-3} for Rh_8Ru_{76}-iter5, but 3.9×10^{-3} for Rh_8Ru_{76}-iter0. The higher θ_{vac} of Rh_8Ru_{76}-iter5 facilitates NH_3 formation by leaving accessible active sites for the N_2 dissociation reaction. In accordance with its higher θ_{vac}, Rh_8Ru_{76}-iter5 has a lower θ_{NH2} (0.73) than Rh_8Ru_{76}-iter0 (0.89). NH_2 is the most abundant adsorbate during NH_3 formation. A high

θ_{NH2} indicates NH_2 poisoning on the surface to reduce the NH_3 formation rate, which is known to be a serious disadvantage of Ru surfaces.[35] Thus, lowering the θ_{NH2} and θ_H values is desirable for the catalytic performance. The present data show that the GAN-generated surface has a lower θ_{NH2} value than those included in the original dataset.

All these results show that the proposed DFT-GAN improves the TOF for NH_3 formation by adjusting the detailed energetics of the elementary reactions. Even though the GAN was not explicitly provided with such information, training the neural networks with DFT data successfully captured these details.

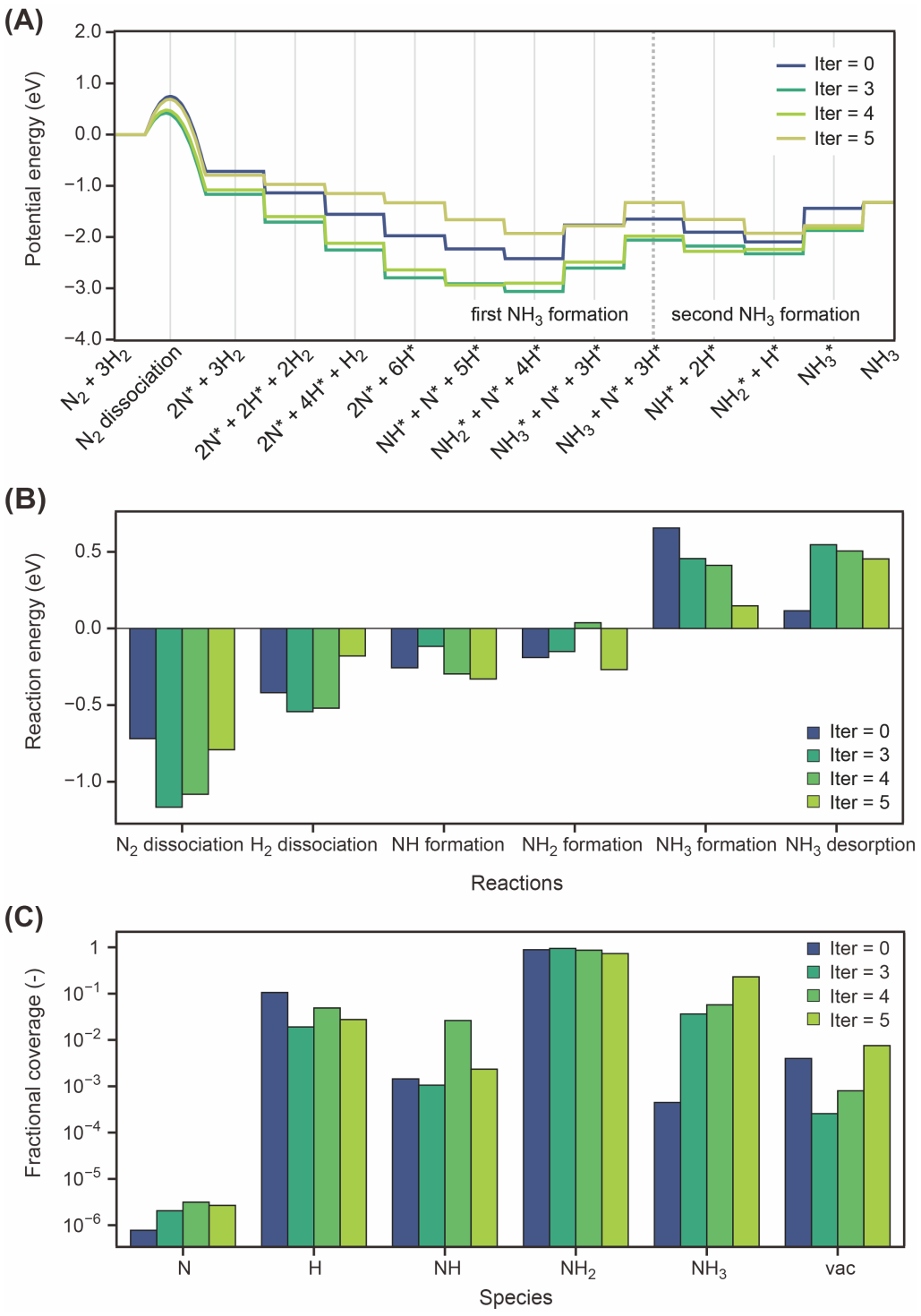

Figure 5. (a) Potential energy profile of NH_3 formation on the Rh-Ru surfaces with the highest TOF at iter 0, 3, 4, and 5. The activation barrier for the RDS (N_2 dissociation) is indicated by the curves on the profile. (b) Reaction energies of the six elementary steps in NH_3 formation over the Rh-Ru surfaces. (b) Coverages of N, H, NH, NH_2, NH_3, and vacant site (vac) on the Rh-Ru surfaces.

4. Conclusions

The present paper proposes a new approach combining computational chemistry and machine learning to generate new catalytic surfaces in an extrapolative manner. Density functional theory (DFT) is used to calculate the energies of elementary reactions on a provided set of catalytic materials. The results are fed into a generative adversarial network (GAN) to propose additional materials. Here, the approach was used to enhance the turnover frequency (TOF) of NH_3 synthesis in the Rh-Ru bimetallic alloy surface system. The DFT-GAN iterations consist of the following steps. (i) DFT is used to obtain the reaction energies (ΔE) of the elementary reactions. This is performed for all surfaces in the initially prepared dataset. (ii) TOF for NH_3 formation is obtained from the ΔE values assuming N_2 dissociation to be the rate-determining step, and the metal surfaces are labeled according to the TOF values. (iii) The GAN consisting of the discriminator and the generator is trained using the above DFT dataset consisting of metal surface information and TOF values. (v) The generator part of the GAN produces fake samples that are not contained in the present dataset. The conditional GAN is used here, and the generator part aims to produce surfaces with higher TOF values. (vi) DFT calculation is performed for the newly generated samples, and the results are added to the dataset.

The iterative process was started with 100 stepped alloy surfaces generated by random atomic replacement. After five iterations, Rh_8Ru_{76} was successfully obtained as a surface not in the original dataset. The TOF of the generated surface was more than ten times higher than the best TOF value in the original dataset. Overall, samples generated in later iterations tend to have higher TOF, indicating that the iterative DFT-GAN scheme helps train the neutral networks in GAN. Also, the generated surfaces generally have a higher proportion of Ru atoms, which agrees with the experimental fact that the Ru surface is a far better catalyst than the Rh surface. The generated surfaces have higher TOF because of (a) a lower N_2 dissociation reaction energy (which reduces activation energy for the rate-determining step) and (b) a lower energy in NH_3 formation (which reduces NH_2 coverage on the surface and alleviates NH_2 poisoning). The present study shows that the combination of DFT and GAN

is a promising strategy for the automatic and continuous improvement of catalyst performance.

Acknowledgements

The author thanks Dr. Yoshitaka Tateyama (National Institute for Materials Science, NIMS) for scientific discussions and assistance with the computational environment. This study was supported by MEXT as an elementary strategy initiative (Grant Number JPMXP0112101003). The calculations were carried out at the supercomputer center of NIMS, Kyushu University (ITO), and Hokkaido University (Grand Chariot).

Supporting Information

The complete dataset (atomic positions, reaction energies, etc.) file is provided.

References

1. Keith, J. A.; Vassilev-Galindo, V.; Cheng, B.; Chmiela, S.; Gastegger, M.; Müller, K.-R.; Tkatchenko, A., Combining Machine Learning and Computational Chemistry for Predictive Insights Into Chemical Systems. *Chem. Rev.* **2021**.

2. Ma, X.; Li, Z.; Achenie, L. E. K.; Xin, H., Machine-Learning-Augmented Chemisorption Model for CO2 Electroreduction Catalyst Screening. *J. Phys. Chem. Lett.* **2015,** *6* (18), 3528-3533.

3. Schlexer Lamoureux, P.; Winther, K. T.; Garrido Torres, J. A.; Streibel, V.; Zhao, M.; Bajdich, M.; Abild-Pedersen, F.; Bligaard, T., Machine Learning for Computational Heterogeneous Catalysis. *ChemCatChem* **2019,** *11* (16), 3581-3601.

4. Zhong, M.; Tran, K.; Min, Y.; Wang, C.; Wang, Z.; Dinh, C.-T.; De Luna, P.; Yu, Z.; Rasouli, A. S.; Brodersen, P.; Sun, S.; Voznyy, O.; Tan, C.-S.; Askerka, M.; Che, F.; Liu, M.; Seifitokaldani, A.; Pang, Y.; Lo, S.-C.; Ip, A.; Ulissi, Z.; Sargent, E. H., Accelerated discovery of CO2 electrocatalysts using active machine learning. *Nature* **2020,** *581* (7807), 178-183.

5. Goldsmith, B. R.; Esterhuizen, J.; Liu, J.-X.; Bartel, C. J.; Sutton, C., Machine learning for heterogeneous catalyst design and discovery. *AIChE J.* **2018,** *64* (7), 2311-2323.

6. Goodfellow, I. J.; Pouget-Abadie, J.; Mirza, M.; Xu, B.; Warde-Farley, D.; Ozair, S.; Courville, A.; Bengio, Y. Generative Adversarial Networks. http://arxiv.org/abs/1406.2661.

7. Mirza, M.; Osindero, S. Conditional Generative Adversarial Nets. https://arxiv.org/abs/1411.1784.

8. Kim, B.; Lee, S.; Kim, J., Inverse design of porous materials using artificial neural networks. *Science Advances* **2020,** *6* (1), eaax9324.

9. Long, T.; Fortunato, N. M.; Opahle, I.; Zhang, Y.; Samathrakis, I.; Shen, C.; Gutfleisch, O.; Zhang, H., Constrained crystals deep convolutional generative adversarial network for the inverse design of crystal structures. *npj Computational Materials* **2021,** *7* (1), 66.

10. Kim, S.; Noh, J.; Gu, G. H.; Aspuru-Guzik, A.; Jung, Y., Generative Adversarial Networks for Crystal Structure Prediction. *ACS Central Science* **2020,** *6* (8), 1412-1420.

11. Dumesic, J.; Rudd, D. F.; Aparicio, L. M.; Rekoske, J. E.; Trevino, A. A., *The Microkinetics of Heterogeneous Catalysis*. ACS Professional Reference Book: Washington DC, 1993.

12. Filot, I. A. W.; Broos, R. J. P.; van Rijn, J. P. M.; van Heugten, G. J. H. A.; van Santen, R. A.; Hensen, E. J. M., First-Principles-Based Microkinetics Simulations of Synthesis Gas Conversion on a Stepped Rhodium Surface. *ACS Catal.* **2015,** *5* (9), 5453-5467.

13. Reuter, K., Ab Initio Thermodynamics and First-Principles Microkinetics for Surface Catalysis. *Catal. Lett.* **2016,** *146* (3), 541-563.

14. Ishikawa, A.; Tateyama, Y., First-Principles Microkinetic Analysis of NO + CO Reactions on Rh(111) Surface toward Understanding NOx Reduction Pathways. *J. Phys. Chem. C* **2018,** *122* (30), 17378-17388.

15. Ishikawa, A.; Tateyama, Y., A First-Principles Microkinetics for Homogeneous–Heterogeneous Reactions: Application to Oxidative Coupling of Methane Catalyzed by Magnesium Oxide. *ACS Catal.* **2021,** *11* (5), 2691-2700.

16. Ertl, G., Surface Science and Catalysis—Studies on the Mechanism of Ammonia Synthesis: The P. H. Emmett Award Address. *Catal. Rev.* **1980,** *21* (2), 201-223.

17. Honkala, K.; Hellman, A.; Remediakis, I. N.; Logadottir, A.; Carlsson, A.; Dahl, S.; Christensen, C. H.; Norskov, J. K., Ammonia Synthesis from First-Principles Calculations. *Science* **2005,** *307* (5709), 555-558.

18. Liu, H., *Ammonia Synthesis Catalysts: Innovation and Practice*. World Scientific / Chemical Industry Press: China, 2013.

19. Dahl, S.; Logadottir, A.; Egeberg, R. C.; Larsen, J. H.; Chorkendorff, I.; Tornqvist, E.; Norskov, J. K., Role of Steps in N2 Activation on Ru(0001). *Phys. Rev. Lett.* **1999,** *83* (9), 1814-1817.

20. Logadottir, A.; Norskov, J. K., Ammonia Synthesis over a Ru(0001) Surface Studied by Density Functional Calculations. *J. Catal.* **2003,** *220* (2), 273-279.

21. Wellendorff, J.; Lundgaard, K. T.; Møgelhøj, A.; Petzold, V.; Landis, D. D.; Nørskov, J. K.; Bligaard, T.; Jacobsen, K. W., Density Functionals for Surface Science: Exchange-Correlation Model Development with Bayesian Error Estimation. *Phys. Rev. B* **2012,** *85* (23), 235149.

22. Blochl, P. E., Projector Augmented-Wave Method. *Phys. Rev. B* **1994,** *50* (24), 17953-17979.

23. Kresse, G.; Furthmuller, J., Efficient Iterative Schemes for Ab Initio Total-Energy Calculations Using a Plane-Wave Basis Set. *Phys. Rev. B* **1996,** *54* (16), 11169-11186.

24. Kresse, G.; Joubert, D., From Ultrasoft Pseudopotentials to the Projector Augmented-Wave Method. *Phys. Rev. B* **1999,** *59* (3), 1758-1775.

25. Norskov, J. K.; Studt, F.; Abild-Pedersen, F.; Bligaard, T., *Fundamental concepts in heterogeneous catalysis*. John Wiley & Sons, Inc.: New Jersey, 2014.

26. Dumesic, J. A.; Trevino, A. A., Kinetic Simulation of Ammonia Synthesis Catalysis. *J. Catal.* **1989,** *116* (1), 119-129.

27. NIST Chemistry WebBook, NIST Standard Reference Database Number 69. https://doi.org/10.18434/T4D303.

28. Norskov, J. K.; Bligaard, T.; Logadottir, A.; Bahn, S.; Hansen, L. B.; Bollinger, M.; Bengaard, H.; Hammer, B.; Sljivancanin, Z.; Mavrikakis, M.; Xu, Y.; Dahl, S.; Jacobsen, C. J. H., Universality in heterogeneous catalysis. *J. Catal.* **2002,** *209* (2), 275-278.

29. Mao, X.; Li, Q.; Xie, H.; Lau, R. Y. K.; Wang, Z.; Smolley, S. P. Least Squares Generative Adversarial Networks. https://arxiv.org/abs/1611.04076v3.

30. Gupta, A.; Zou, J., Feedback GAN for DNA optimizes protein functions. *Nature Machine Intelligence* **2019,** *1* (2), 105-111.

31. Dong, Y.; Li, D.; Zhang, C.; Wu, C.; Wang, H.; Xin, M.; Cheng, J.; Lin, J., Inverse design of two-dimensional graphene/h-BN hybrids by a regressional and conditional GAN. *Carbon* **2020,** *169*, 9-16.

32. Ask Hjorth, L.; Jens Jørgen, M.; Jakob, B.; Ivano, E. C.; Rune, C.; Marcin, D.; Jesper, F.; Michael, N. G.; Bjørk, H.; Cory, H.; Eric, D. H.; Paul, C. J.; Peter Bjerre, J.; James, K.; John, R. K.; Esben Leonhard, K.; Joseph, K.; Kristen, K.; Steen, L.; Jón Bergmann, M.; Tristan, M.; Thomas, O.; Lars, P.; Andrew, P.; Carsten, R.; Jakob, S.; Ole, S.; Mikkel, S.; Kristian, S. T.; Tejs, V.; Lasse, V.; Michael, W.; Zhenhua, Z.; Karsten, W. J., The Atomic Simulation Environment—A Python Library for Working with Atoms. *J. Phys.: Condens. Matter* **2017,** *29* (27), 273002.

33. Ishikawa, A. Github. https://github.com/atsushi-ishikawa.

34. Ozaki, A.; Aika, K.-i.; Hori, H., A New Catalyst System for Ammonia Synthesis. *Bull. Chem. Soc. Jpn.* **1971,** *44* (11), 3216-3216.

35. Ishikawa, A.; Doi, T.; Nakai, H., Catalytic Performance of Ru, Os, and Rh Nanoparticles for Ammonia Synthesis: A Density Functional Theory Analysis. *J. Catal.* **2018,** *357*, 213-222.
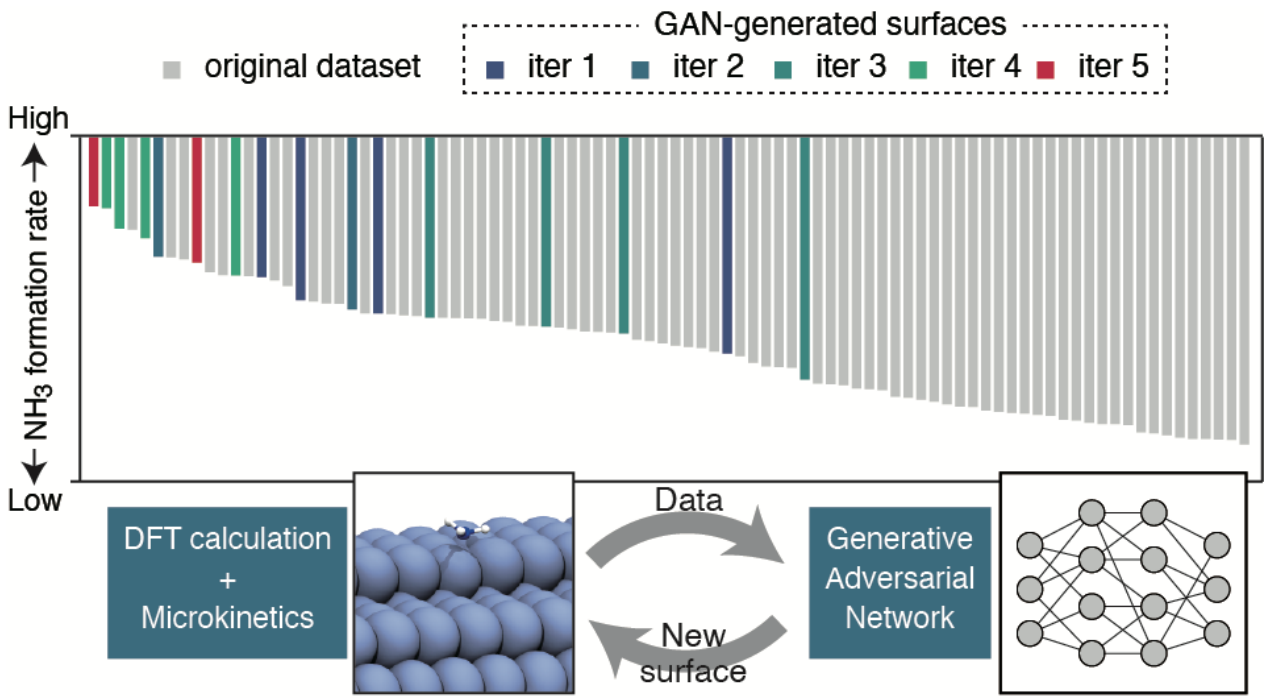
Table of contents figure